Chemosphere 365 (2024) 143327

Contents lists available at ScienceDirect

Chemosphere

journal homepage: www.elsevier.com/locate/chemosphere

Anelosimus eximius bioinspired ZnO nano cobwebs for environmental remediation of drugs and endocrine disruptors from water

Milan Masar [a], Hassan Ali [a], Muhammad Yasir [a], Barbora Hanulikova [a], Orhan Sisman [b], Michal Zitnan [b], Michal Machovsky [a,*], Jose J. Velazquez [b], Dusan Galusek [b,c], Ivo Kuritka [a]

[a] Centre of Polymer Systems, Tomas Bata University in Zlin, Tr. T. Bati 5678, 76001, Zlin, Czech Republic
[b] Centre for Functional and Surface Functionalized Glass, Alexander Dubček University of Trenčín, Študentská 2, SK-911 50, Trenčín, Slovakia
[c] Join Glass Centre of the IIC SAS, TnU AD, and FChPT STU, Trenčín, Slovakia

HIGHLIGHTS

- *Anelosimus eximius* bioinspired ZnO-based nanorods/nano cobweb grown onto substrate.
- Secondary ZnO cobweb-like structure increases primary ZnO nanorods hydrophilicity.
- Ag deposition onto ZnO nanostructures was achieved by photoreduction method.
- Total degradation of E3 hormone was achieved in a continuous flow photoreactor.
- Reusability of the immobilized photocatalyst was determined after five cyclic runs.

GRAPHICAL ABSTRACT

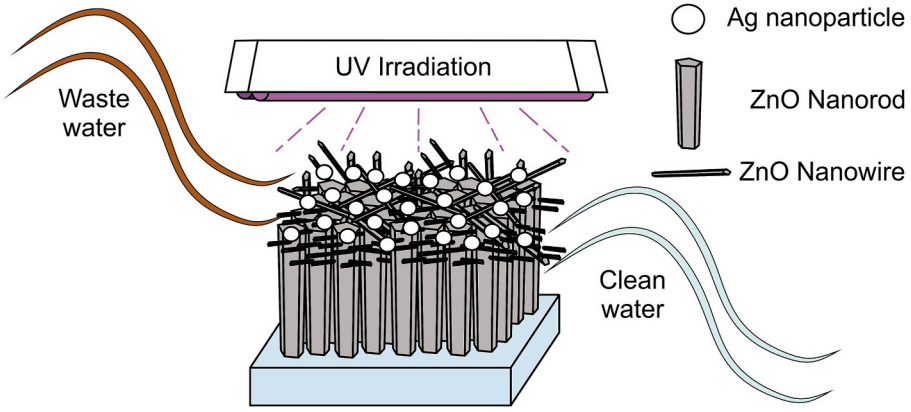

ARTICLE INFO

Handling editor: Vicente Rodríguez-González

Keywords:
ZnO
Silver nanoparticle
Photocatalysis
Water treatment
Estrogens
Drugs

ABSTRACT

The pollution of wastewater with pharmaceuticals and endocrine-disrupting chemicals (EDCs) in populated areas poses a growing threat to humans and ecosystems. To address this serious problem, various one-dimensional (1D) hierarchical ZnO-based nanostructures inspired by Anelosimus eximius cobwebs were developed and successfully grown on a glass substrate through simple hydrothermal synthesis. The nanorods (nr) obtained during primary growth were chemically etched with KOH (ZnO_{nr}-KOH), followed by the secondary growth of nano cobweb-like (ncw) structures using polyethyleneimine ($ZnO_{nr/ncw}$). These structures were further decorated by the photoreduction of Ag nanoparticles ($ZnO_{nr/ncw}$/Ag). The feasibility of ZnO-based 1D nanostructures to remove pollutants was demonstrated by degrading commonly prescribed pharmaceutical drugs (diclofenac and carbamazepine) in a miniature cuvette reactor. The photocatalytic activities for drug degradation generally decreased in the order $ZnO_{nr/ncw}$/Ag > $ZnO_{nr/ncw}$ > ZnO_{nr}-KOH. Additionally, the suitability of the samples for scaling up and practical application was demonstrated by photocatalytic degradation of the hormone estriol (E3) in a flow-through photoreactor. The photocatalytic degradation efficiency of E3 followed the same trend

* Corresponding author.
E-mail address: machovsky@utb.cz (M. Machovsky).

https://doi.org/10.1016/j.chemosphere.2024.143327
Received 3 April 2024; Received in revised form 28 August 2024; Accepted 10 September 2024
Available online 11 September 2024

observed for drug degradation, with the complete elimination of the endocrine disruptor achieved by the best-performing $ZnO_{nr/ncw}$/Ag within 4 h, due to optimized charge transfer and separation at the heterostructure interface.

1. Introduction

Ever-increasing population growth and industrialization have exacerbated environmental pollution and energy crises, negatively impacting humans and the planetary ecosystem. Over the last few decades, various synthetic chemical effluents have been released on an industrial scale without proper remediation. These environmental pollutants have been classified into multiple categories, with each having a relative degree of potential biotoxicity, such as organic dyes, pesticides, pharmaceutical drugs, dioxins, biological hazards, endocrine disruptors (EDCs), and polychlorinated biphenyls (Haddaoui and Mateo-Sagasta, 2021). Particular concerns have been raised for EDCs, a class of toxicants that have been present in the environment for decades. However, their toxicity has only recently been determined due to advancements in pathophysiological pathways. EDCs are known to potentially disrupt the endocrine system in mammals, including humans, which controls various physiological functions such as metabolism and sexual development. The current scientific consensus is that increased concentration and exposure to different environmental toxicants are correlated with higher incidence rates of various diseases such as leukemia, cancers, neurological diseases, and metabolic disorders (Ghosh et al., 2022). Moreover, EDCs are highly biotoxic and bioaccumulative, even at minuscule concentrations of a sub-nanogram scale. EDCs are ubiquitous as they are found in nearly all everyday household items, mostly in personal care and hygiene products, plastics, food storage, sunscreens, Teflon, nonstick wrappers, electronics, and building materials (Choi et al., 2004; Kumar et al., 2020). Some common EDCs in the environment are bisphenol A, perchlorate, phthalates, perfluoroalkyl and polyfluoroalkyl substances, and estrogenic hormones (Rhomberg et al., 2014). Additionally, excessive use of pharmaceutical drugs causes their discharge into water streams without prior remediation, negatively impacting biodiversity due to their relatively high biopotency (Ortúzar et al., 2022). Therefore, several regulatory agencies have introduced guidelines establishing thresholds for various pollutants. Considering these environmental risks, current research efforts are devoted to wastewater remediation before its subsequent discharge into the environment.

So far, various techniques have been investigated, such as membrane technology, ozonation, reverse osmosis, adsorptive process, biological degradation, and photocatalysis (Grzegorzek et al., 2023; Nure and Nkambule, 2023). Among these, photocatalysis has emerged as a highly effective strategy for wastewater treatment due to its relative ease of operation, energy-cost benefits, and low degree of secondary pollution (Mishra et al., 2023; Moeen et al., 2022). In addition to typical wastewater treatment, photocatalysts exhibit additional advantages of antibacterial performance (Ayesha et al., 2023; Ikram et al., 2023). However, intrinsic materials lack sufficient photocatalytic activity due to the futile recombination of excitons and the restricted availability of active sites. Considering this, photocatalytic materials are usually modified with metallic particles (Pham et al., 2023), formation of heterojunction (Sharma et al., 2024), and decoration with noble metals (Semalti et al., 2023) to achieve synergistic effects resulting in enhanced charge transfer which in turn increases the overall photocatalytic efficiency (Shaheen et al., 2024; Shahzadi et al., 2023).

ZnO is considered a well-known and preferred choice for photocatalytic applications due to its wide bandgap, biocompatibility, and facile synthesis methods (Preeti et al., 2023). For example, Ricardo's group utilized ZnO as a base component of different multicomponent photocatalytic systems for advanced applications with a significant leap in performance (Gil et al., 2020; Manríquez et al., 2017; Piña-Pérez et al., 2018). However, ZnO, like other photocatalytic materials, suffers from low efficiency in the practical and real implementation of photocatalytic applications. Therefore, various ingenious design strategies have been developed to improve electron-hole transport, backward charge recombination, and degree of light absorption spectrum (Li et al., 2022). Interestingly, photocatalysts can be imparted with a significant increase in photoactivity solely by engineering various aspects of intrinsic structural features. These features primarily include surface area, exposed facets, relative crystallinity, and variation in particle size distribution, all of which directly influence charge transfer (Kusiak-Nejman et al., 2023). Fortunately, developing biomorphic nanostructured photocatalysts inspired by natural organisms is a compelling way to achieve such structural features. Various bioinspired photocatalysts have been developed to impart enhanced light absorption, charge separation, and structural integrity (Yang et al., 2022). For example, Fan et al. fabricated a ternary CdS/Au/TiO_2 photocatalyst resembling butterfly wings, known for their antireflection and high light absorption capability (Ding et al., 2013). By replicating nanostructural motifs of *Papilio nephelus Boisduva* butterfly wings, Fan's group was able to achieve UV reflection reduced by 40% according to finite-difference time-dome (FDTD) simulation while their photocatalytic efficiency improved up to 200% compared with reference TiO_2 configuration (Ding et al., 2013). Similarly, phototropic structures maximizing light absorption found in various plants, particularly sunflowers, have also been replicated with excellent results (Qin et al., 2021). By taking inspiration from spider webs, significant structural strength can be imparted while reducing the costs of fabricating photocatalytic materials. Moreover, spider silk possesses dual hydrophobic and hydrophilic characteristics which can be contrived for ZnO nanostructures for self-cleaning applications (Nundy et al., 2020; Römer and Scheibel, 2008). Besides modulating the intrinsic features of a photocatalyst, the physical decoration of a photocatalyst with metallic nanoparticles has been considered a well-established strategy for improving photocatalytic activity (Shandilya et al., 2022). The overall charge dynamics can be significantly enhanced even for bare photocatalytic materials by optimizing their structural properties and morphology, especially the aspect ratio (Ganguli et al., 2022; Masar et al., 2024). Considering geometric aspects, one-dimensional (1D) photocatalytic materials, including ZnO, have shown great potential due to their unique morphology features. A high aspect ratio shortens the diffusion path length, resulting in efficient charge carrier separation and high provision of active sites (Perdomo and Nguyen, 2022). For example, Ocon et al. synthesized a multidimensional ZnO in 0D (nanoparticle), 1D (nanorod), 2D (nanosheet), and 3D (nanoflowers) configurations via highly controlled state-of-the-art synthesis methods. Among the synthesized configurations, 1D ZnO nanorods exhibited a superior photodegradation rate of 99.4% for salicylic acid and the highest bactericidal activity for *B. subtilis* and *E. coli.* The high activity of 1D ZnO nanorods was attributed to enhanced physicochemical properties, i.e., small crystallites, specific surface area, and pore diameter (Chang et al., 2020). Besides tailoring morphology, pristine photocatalytic materials are often decorated with metallic nanoparticles to achieve localized surface plasmon resonance (LSPR) (Lv et al., 2022). For instance, Jiada et al. reported on a facile hydrothermal synthesis of ZnO–Au nanocomposites. The ZnO nanorods decorated with Au nanoparticles performed exceptionally well with the rate constant of $\sim k = 1.19 \times 10^{-2}\,min^{-1}$ in comparison to bare ZnO nanorods ($\sim k = 6.36 \times 10^{-4}\,min^{-1}$) for rhodamine blue dye photodegradation. The high activity was ascribed to suppressed charge recombination and extended light absorption due to the incorporation of Au nanoparticles (Yao et al., 2021). Besides the LSPR effect manifested

only under specific conditions, noble metal nanoparticles decorated onto semiconductor photocatalysts also act as electron sinks, effectively boosting charge carrier separation (Petryayeva and Krull, 2011). Particularly, Babel et al. reported that metallic Ag tends to increase the electron population of ZnO, inhibiting charge recombination. The photoexcited electrons in ZnO were restricted from recombination with the complementary holes by migrating to the Ag metal loaded on the host ZnO and were thus spatially separated from the holes. In this scheme, the Ag metal acts as an electron sink, enhancing photoactivity (Sudrajat and Babel, 2019).

In this work, we report on the design of 1D nanostructured ZnO possessing nanorods/nano cobweb geometric configurations resembling *Anelosimus eximius* spider cobwebs grown onto a glass substrate. The secondary growth of ZnO nano cobwebs achieved by etching the primary growth of ZnO nanorods and varied polyethyleneimine (PEI) molecular weight can be eventually followed by silver (Ag) nanoparticles decoration via the photoreduction method. The novelty of this work derives from the fabrication of structurally preferred ZnO nanostructures, which can be obtained by primary and secondary growth using varied PEI molecular weights as a capping agent during the growing phase. The suitability of samples for water treatment was demonstrated by photodegradation of two commonly prescribed drugs, carbamazepine and diclofenac, and estriol (E3) hormone as a model EDC pollutant. Carbamazepine and diclofenac water solutions were degraded in a self-designed experimental setup comprising a Cary 300 UV–visible spectrophotometer equipped with householder for 3 UV LEDs miniature cuvette photoreactor. The degradation of the E3 hormone in a continuous flow UV photoreactor evinced the feasibility of scaling up as well as reusability study. Besides their application in water treatment, self-cleaning capability was demonstrated based on surface photocatalytic activity assessment and a wettability study.

2. Materials and methods

All experimental preparation methods, characterization techniques, and materials utilized throughout the study are comprehensively described in section 1 of the provided supplement document. Summarily, ZnO samples with specific nanostructured morphologies were prepared via the hydrothermal method, while obtained ZnO samples were further decorated with Ag using the photoreduction method, as shown in

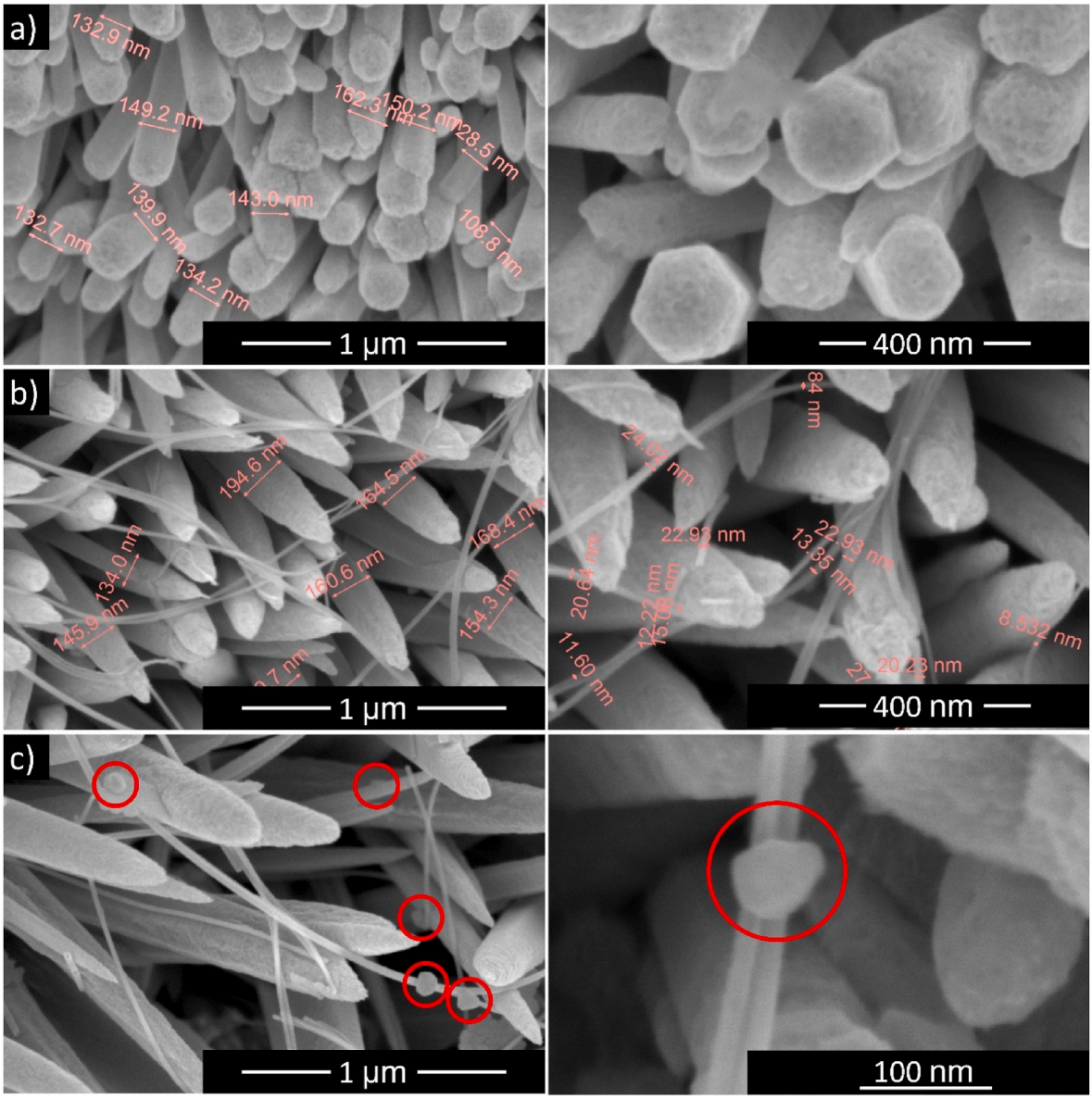

Fig. 1. Detailed SEM images of samples ZnO_{nr}-KOH (a), $ZnO_{nr/ncw}$ (b), and silver decorated sample - $ZnO_{nr/ncw}$/Ag (c).

Fig. S1. Labelling of all samples along with their description are highlighted in Table S1. Photodegradation studies of diclofenac sodium salt, carbamazepine, and estriol were obtained using UV–vis and liquid chromatography. A schematic illustration of the utilized experimental setup is given in Fig. S2.

2.1. SEM analysis

The morphology of as-prepared samples was examined by SEM as shown in Fig. 1a–c, with adjacent images corresponding to associated high-resolution images. A highly oriented and mostly uniform ZnO with nanorods configuration was observed for all samples. The obtained ZnO_{nr} sample was etched with KOH solution for 30 min to induce secondary growth. (Fig. 1a). The nanorods in the etched sample exhibit a slight overall shrinkage while maintaining a homogenous appearance. The KOH etching induced the formation of a porous ZnO surface. The porous sites on KOH-etched ZnO_{nr} could act as a seed layer inducing the secondary growth of the ZnO nanorods (Fig. 1b) (Ching et al., 2013). As can be seen in Fig. 1b, the mentioned secondary growth consists of fine thread-like ZnO structures with horizontal orientation that formed a webbed structure on the top of ZnO nanorods. It should be noted that each threaded ZnO structure appears to be physically connected with the primary ZnO nanorods, which is particularly useful for immobilization of the substrate. Literature reports suggest that an increase in pH is a factor that induces structural and optoelectronic variations during the initial growth. Since the pH during this process was increased from 7.6 to 8.1 by the incorporation of PEI, the growth of nano cobweb-like ZnO structures rather than nanorods could be attributed to pH variation (Abdulrahman et al., 2021). However, PEI is also a chelating agent for many heavy metal ions, including Zn(II) (Ayalew et al., 2022). Therefore, besides sudden changes in pH, it may also effectively lower the concentration of Zn(II) in the chemical bath. A lower concentration of Zn (II) in a chemical bath is well recognized to enable the thinning of 1-D ZnO nanostructures and increase aspect ratio. For instance, ultralong 40 μm ZnO nanowires were grown, which is ascribed to a lower concentration of precursor in a chemical bath (Qiu et al., 2010). The obtained ZnO nanorods/nano cobweb-like sample was further decorated with Ag nanoparticles, as shown in Fig. 1c. Briefly, the sample appears to have the main characteristic features of the first and secondary growth of ZnO nanorods and nano cobwebs. At the same time, small Ag particles can be seen lodged uniformly in the nanostructured ZnO.

2.2. XRD analysis

The crystal structures of all as-prepared samples were characterized by XRD and the corresponding diffractograms are shown in Fig. 2A. For reference, the XRD pattern of blank glass (BG) is also given, exhibiting no signs of crystalline and/or semi-crystalline impurities (Fig. 2A). For all ZnO samples, the main characteristic peaks are observed at diffraction angles 2θ of 37.02°, 40.19°, and 42.32°, which are ascribed to the diffraction planes (100), (002), and (101) of hexagonal wurtzite phase of ZnO structure, in accordance with the PDF card No. 01-073-8765. Moreover, the proportion between main characteristic peaks remains almost unchanged for all samples, with the most pronounced reflections observed for the (002) plane indicating the presence of ZnO nanorods preferentially oriented perpendicularly to the substrate surface. The presence of nano cobweb configurations does not change the diffractogram patterns significantly. However, Fig. S3 in the supplement, which provides an enlarged view for triade of the most prominent peaks, including maxima positions of diffraction angles and FWHW values, indicates certain changes in microstructure for etched sample ZnO_{nr}-KOH. Compared to cobweb-decorated ZnO nanostructures, the etched sample exhibits a larger value of FWHM, while the peak maxima position does not change significantly. Average crystallite domain size was estimated by the Halder-Wagner method for ZnO_{nr}-KOH, $ZnO_{nr/ncw}$, and $ZnO_{nr/ncw}$/Ag to be (36.7 ± 0.2 nm), (39.7 ± 0.1 nm), and (37.8 ± 0.2 nm), respectively (Nath et al., 2020). Accordingly, corresponding lattice strain values were evaluated to be 0.08 ± 0.006 %, 0.03 ± 0.001 %, and 0.08 ± 0.003 % for ZnO_{nr}-KOH, $ZnO_{nr/ncw}$, and $ZnO_{nr/ncw}$/Ag, respectively. The physical decoration of the Ag nanoparticles was confirmed for the sample $ZnO_{nr/ncw}$/Ag showing additional peaks at the diffraction angles 2θ of 44.56, 52.29, and 77.09° corresponding to the diffraction planes of (111), (200), and (220) of Ag, respectively (PDF Card No. 01-077-6577). The characteristic peaks of Ag with a crystalline domain size of 10.9 ± 0.2 nm observed for the Ag/ZnO nanocomposite were in accordance with the literature reports (Liu et al., 2019a).

2.3. Raman spectroscopy

The Raman spectra of as-prepared samples, including the blank glass, are shown in the right panel in Fig. 2B. The bands in the spectra marked in grey belong to Raman shifts of the glass, where the smaller sharp band around 474 cm^{-1} is attributed to the vibrationally isolated Si–*O*–Si mode. The 583 cm^{-1} band may be attributed to the symmetric stretching vibration of the Si–O bond, while the 1099 cm^{-1} band can be assigned to the asymmetric Si–O stretching vibration of SiO_4 tetrahedra (Yadav and

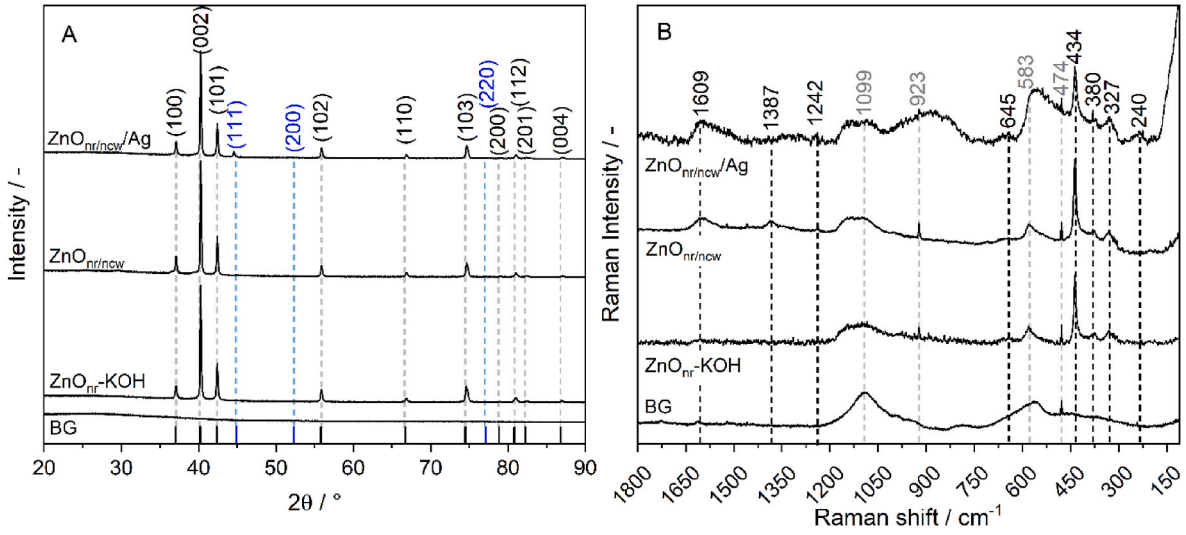

Fig. 2. XRD patterns (A) and Raman spectra (B) for prepared samples.

Singh, 2015). The 923 cm^{-1} band is attributed to a Si–O stretching vibration with two nonbridging O atoms per silicon atom (Manghnani et al., 2011). The intense band at 434 cm^{-1} corresponds to the non-polar E2 (high) mode, which originates from the oxygen vibration in ZnO and indicates its highly crystalline wurtzite structure (Ansari et al., 2018; Ribut et al., 2019). The band at 380 cm^{-1} and the smaller band at 330 cm^{-1} show the vibrational symmetric A1 (TO) mode due to multiple phonons scattering (Hansen et al., 2019). The low-intensity band at 327 cm^{-1} is related to the second-order Raman spectrum arising from phonons at the hexagonal ZnO zone boundary, labeled as E2 (high) - E2 (low) (Ribut et al., 2019). Another prominent band at 583 cm^{-1} associated with E1 (LO) mode was recorded, indicating the presence of oxygen vacancies, zinc interstitials, and their complexes (Sawant et al., 2018). Similarly, a band at around 240 cm^{-1} was detected, which can be attributed to the silent, inactive B1 mode in the ZnO structure or the plasma lines of the laser used. In general, the presence of Ag nanoparticles was observed to affect the signal intensity of Raman shifts (Sawant et al., 2018), while all Raman active modes were detected for all samples without any ambiguity. The obtained Raman analysis is in accordance with other literature reports on ZnO (Musa et al., 2017) nanostructures and indicates absence of any impurity phases, corroborating XRD analysis.

2.4. XPS analysis

The XPS survey scans extended up to the binding energy of 1350 eV are shown in Fig. 3 left. The high-resolution XPS spectra were recorded to analyze the chemical states of Zn, Ag, and O. The Zn $2p_{3/2}$ and Zn $2p_{1/2}$ peaks (Fig. 3, right) are located around 1021.6 and 1044.6 eV, respectively, corresponding to splitting of 23.0 eV, suggesting the existence of Zn^{2+} lattice ions (Moulder and Chastain, 1992; National Institute of Standards and Technology, 2000). No shift in the binding energies is observed when the Zn 2p satellite curves are compared, indicating that Ag was loaded on the surface of $ZnO_{nr/ncw}$. In Fig. S4, two peaks associated with Ag are observed at 373.1 eV and 367.1 eV corresponding to Ag $3d_{5/2}$ and Ag $3d_{3/2}$, respectively. The splitting of 6.0 eV in the 3d doublet confirms the metallic nature of silver present on the surface of $ZnO_{nr/ncw}$/Ag. The measured spectra shifted about 0.9 eV towards lower binding energy compared with the corresponding values of pure metallic Ag^0 (368.2 eV and 374.2 eV) (Moulder and Chastain, 1992; Zhu et al., 2023). The shift of binding energy of Ag 3d corresponds to the electron transfer from metallic Ag nanoparticle decorations to $ZnO_{nr/ncw}$, as was observed previously for Ag/ZnO heterojunctions (Bazant et al., 2015; Chen et al., 2011; Lin et al., 2009; Liu et al., 2019b).

In addition, no peak is observed in Fig. S5 at the binding energy below 530 eV (such as 529.0 eV, which is attributed to lattice O in Ag_2O and suggests the presence of silver as Ag^0 (Mou et al., 2018). Although the de-convolution of O (1s) peaks (Fig. S5) is rather semiquantitative, it still has an instructive value. The de-convoluted peaks for all ZnO_{nr}-KOH, $ZnO_{nr/ncw}$, and $ZnO_{nr/ncw}$/Ag exhibit similar binding energies and are typically classified as crystal lattice oxygen (O_1), the surface oxygen vacancy (O_2) and surface oxygen species (O_3). Recently, Frankcombe and Liu proposed that O_2 peak is not related with oxygen vacancy (Frankcombe and Liu, 2023), associating it with the O 1s electrons from water molecules strongly bound to the exposed ZnO surface or surface oxygen passivated with hydrogen. Hicham Idriss pointed out, that assignment of the O (1s) signal at 531–532 eV attributed to oxygen vacancies cannot be rigorously performed on powder oxides exposed to ambient conditions (Idriss, 2021). Krzywiecki et al. examined the construction of a band diagram of ZnO analyzing in-depth photoemission spectra in combination with Kelvin probe data and highlighted the discrepancy between theoretical studies and experimental findings (Krzywiecki et al., 2015). In addition to the probability of donor states originating from the oxygen vacancies and coordinatively unsaturated anion O^{2-} related to oxygen or water vapor, they proposed that the morphological features (column-like) can also be effective in the formation of morphology-related trap states that arose from oxygen vacancies which sounds plausible in the case of our ZnO nanorod samples (Krzywiecki et al., 2015). An advanced, in-depth surface analysis, which is beyond the scope of this study, may help to elucidate the (O_2) peak precisely. Besides, a notable decrease in surface oxygen (O_3) concentration can be observed in the $ZnO_{nr/ncw}$/Ag sample compared to the bare $ZnO_{nr/ncw}$ sample. A relative increase of surface vacancies in contrast to surface oxygen can enhance adsorption and photocatalytic reactions, as observed in the $ZnO_{nr/ncw}$/Ag sample (Chen et al., 2011; Lin et al., 2009; Liu et al., 2019b). In addition, a direct correlation between oxygen vacancies and increased light absorption has been established as per literature reports, which potentially corroborates the optimized photocatalytic performance of the $ZnO_{nr/ncw}$/Ag sample (Han et al., 2009). On the other hand, the surface oxygen species are commonly associated with hydroxyl groups. Extended XPS analysis data including peak assignment, position, and FWHM of all samples are provided in Table S2.

2.5. Qualitative photocatalytic assessment and wettability evaluation

A preliminary qualitative analysis according to ISO standard No. 21066:2018 and wettability evaluation as a measure of the self-cleaning

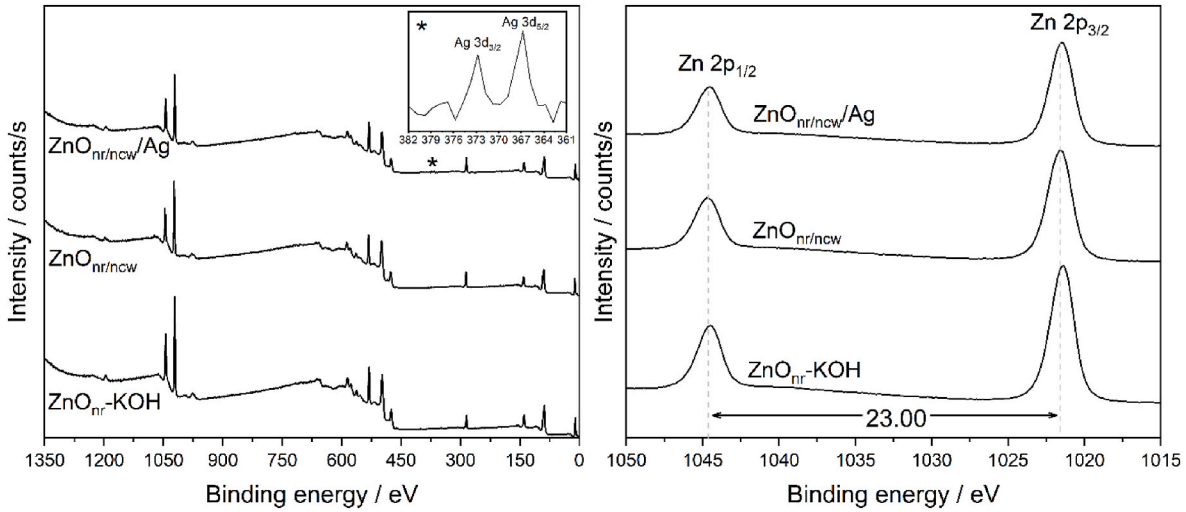

Fig. 3. Extended XPS spectra of as-prepared samples with Ag 3d peaks in the inset (left) and zoomed-in spectra for Zn 2p signals (right).

ability of all samples were evaluated comprehensively as it can indicate high photocatalytic performance in relevant applications. The obtained experimental results are described in supplement sections 2.3 and 2.4, respectively.

2.6. Photodegradation of diclofenac and carbamazepine

The selected pharmaceutical drugs were used to determine the photocatalytic activity of the prepared samples and photodegradation rate constants of diclofenac and carbamazepine at concentrations of 6.125 mg/L in demi-water solution. The samples were measured using an online apparatus, where each sample was placed on the side of a fluorescence cuvette filled with 3 mL of drug solution and uniformly illuminated by LEDs. The absorbance of each drug was recorded at regular intervals. In this setup, the need for sampling is eliminated; thus, no influence can arise due to slight variations in concentration. The samples were measured at 1 h intervals until the experiment was terminated after 5 h. The obtained results for the degradation of diclofenac and carbamazepine are given in Fig. 4. Photodegradation followed pseudo-first-order kinetics with the rate constant calculated according to the following equation:

$$-\ln\left(\frac{c_t}{c_0}\right) = kt \quad (1)$$

where c_0 is the concentration of the drug solution at the start of the reaction, c_t is the concentration at a chosen time interval, t and k are the photodegradation reaction rate and kinetic constant, respectively. The obtained rate constants are given in Table S5. Blank samples exhibit almost negligible photodegradation for both drugs under UV irradiation, indicating that model drugs used in the study have almost no self-photodegradation. The structural stability and lack of self-photosensitization are essential issues when evaluating synthetic organic pollutants. From the results, the trend for photocatalytic degradation achieved for both drugs is as follows: $ZnO_{nr/ncw}/Ag$ > $ZnO_{nr/ncw}$ > ZnO_{nr}-KOH. For the sample ZnO_{nr}-KOH, low photocatalytic activity is observed, which could be attributed to the alteration of surface chemistry for the photocatalytic reaction due to the etching procedure. Moreover, it should be noted that average crystalline domain sizes estimated by XRD (section 2.2) do not change significantly after etching further implying that solely surface chemistry alteration impacted photocatalytic performance (see Fig. 1A). A similar effect of KOH etching accompanied by significant changes in morphology and crystal structure has been reported for ZnO by other authors, (El-Shaer et al., 2018; Ranjith et al., 2013). For instance, Mosaad et al. reported that etching by KOH at high molarity resulted in a change in the size of ZnO crystallites and decreased crystallinity (El-Shaer et al., 2018). In the case of morphology-optimized $ZnO_{nr/ncw}$, the photodegradation is significantly improved for both drugs, possibly due to enhanced surface quality of secondary-grown structural features and their crystalline uniformity. The highest photocatalytic degradation was observed for the $ZnO_{nr/ncw}/Ag$ heterojunction sample, in which photodegradation rate constants of 22.3×10^{-4} min^{-1} and 28.2×10^{-4} min^{-1} were achieved for diclofenac and carbamazepine, respectively. The optimized activity of the Ag-decorated ZnO sample can be ascribed to the optimized separation of charge carriers, in which Ag metallic particles act as electron sinks and drive away the photogenerated electrons from holes. In this way, electrons and holes can initiate photocatalytic reactions instead of undergoing futile charge recombination (Sudrajat and Babel, 2019). Besides ZnO, such separation of charge carriers has also been reported in other metallic nanoparticle-decorated systems (Gao et al., 2017; Majeed et al., 2022). It should be noted that the degradation rate of carbamazepine (M_w = 236.26 g/mol) is higher in comparison to diclofenac (M_w = 318.13 g/mol), which could be due to relative difference in molecular weight and reduced molecular cleavage. The molecular weight of individual pollutants has been associated with an inverse photocatalytic trend, i.e., increased molecular weight leads to decreased photocatalytic degradation (Kalaiarasan et al., 2021). Diclofenac has a pKa value of 4.2, which implies a negative charge of the molecule at neutral pH. On the other hand, carbamazepine has pKa_1 and pKa_2 values of 2.3 and 13.9, respectively, which implies a neutral charge at neutral pH and complies with lower solubility compared with diclofenac (Ensano et al., 2017). The photocatalytic degradation pathway is primarily based on numerous reactive oxygen species (ROS) that are produced by photoexcited electron-hole pairs in an aqueous medium. According to the literature reports, the main reactive species responsible for the photodegradation of carbamazepine are $^{\bullet}OH$ and $O_2^{\bullet-}$ which target the molecules generating various byproducts (Durán et al., 2016). In the case of diclofenac, the main species were found to be oxidative holes (either directly or by subsequent generation of $^{\bullet}OH$, confirmed via photoluminescence spectra using terephthalic acid (TA) as a probe molecule (Mugunthan et al., 2019).

2.7. Photodegradation of estriol hormone

The photodegradation of estriol (E3) hormone was used as a model endocrine disruptor to demonstrate further the capability of developed photocatalytic thin films. The molecular weight of the E3 hormone is 288.38 g/mol, which is in the range of the other two evaluated drugs, so the results can be expected to be comparable. The as-obtained samples of photocatalytic films were evaluated using Drip Flow Biofilm Reactor

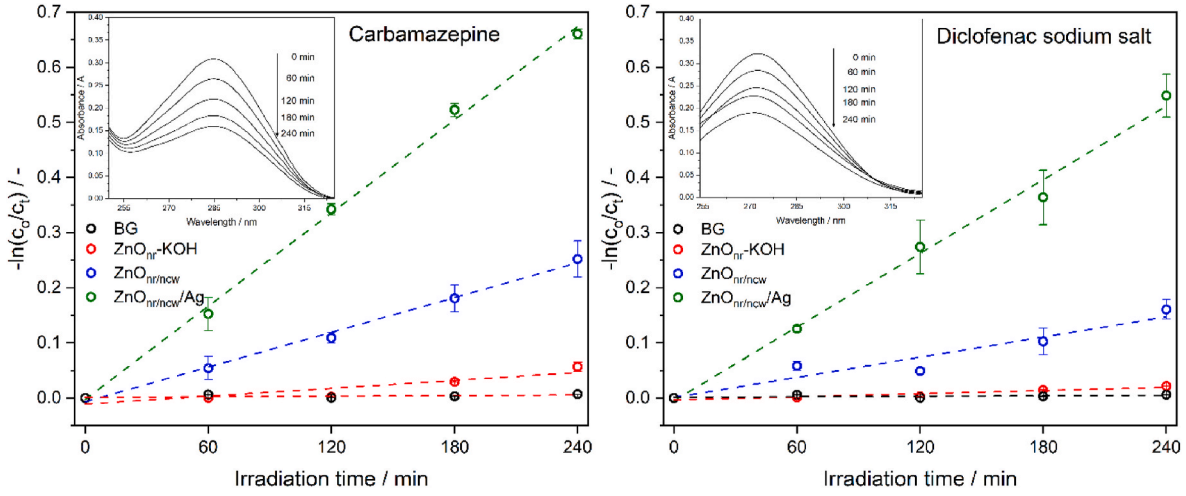

Fig. 4. Pseudo-first-order kinetics plots of photodegradation of carbamazepine (left) and diclofenac sodium salt (right).

DFR 110-4PET, which consists of four channels. The samples were placed in each channel and irradiated using an external UV lamp mounted directly above the samples, while a continuous flow of E3 solution (0.3 mg/L) was circulated through the photoreactor using a peristaltic pump equipped with silicon tubing. For all experiments, a constant flow rate of 12 mL/min was set to minimize any fluctuations due to residence time. It is pertinent to mention that the photocatalytic reaction rate depends strongly on the flow rate, i.e., gradually increasing the flow rate boosts the photocatalytic rate until an optimum is reached, which is the maximum photocatalytic rate dependent on the flow rate (García-Prieto et al., 2022). The percentual removal of E3 by photodegradation at each 1 h interval for a total duration of 4 h is graphically shown in Fig. 5, left. The same relative trend is obtained for the photodegradation of E3 of all samples, i.e., $ZnO_{nr/ncw}/Ag > ZnO_{nr/ncw} > ZnO_{nr}$-KOH. The trend shows an increase in photodegradation of E3 hormone from 38% to 99.4%, 18.7%–74.2%, and 0.9%–43.3% for $ZnO_{nr/ncw}/Ag$, $ZnO_{nr/ncw}$, and ZnO_{nr}-KOH, respectively, in the time interval between first and fourth hour. The $ZnO_{nr/ncw}/Ag$ sample shows much higher photocatalytic activity than the sample $ZnO_{nr/ncw}$ without Ag decoration, confirming the heterojunction effect. The results indicate that $ZnO_{nr/ncw}/Ag$ can almost completely degrade E3 hormone in the given time compared to $ZnO_{nr/ncw}$ and ZnO_{nr}-KOH, which were able to eradicate only 74.2% and 43.3% of the hormone, respectively. The obtained results are similar to those found in the literature studies on ZnO photocatalysts for E3 degradation. For example, Gao et al. reported a total E3 degradation rate of 95% at 0.6 mg/L concentration within an hour using 10 mg/L of pristine ZnO (Al-Hajji et al., 2021; Han et al., 2012). However, their developed system was tested in a slurry-based reactor, which can result in secondary pollution due to poor recoverability in contrast to the as-obtained immobilized system developed in this study, which offsets the slightly increased performance of slurry-based systems.

Scavenger tests were performed using the $ZnO_{nr/ncw}$ sample with the same preset experimental conditions to elucidate further the role of active species initiating the photocatalytic reaction. In particular, disodium ethylenediaminetetraacetate (EDTA), *tert*-butyl alcohol (TBA), and 1,4-benzoquinone (PBQ) were employed for quenching holes, $^{\bullet}OH$, and $^{\bullet}O^{2-}$, respectively. The obtained results (Fig. 5, right) revealed that with the introduction of EDTA and TBA, a significant decrease in the photocatalytic activity was observed for both recorded 1 h intervals. It can be inferred that both holes and $^{\bullet}OH$ radicals were the main reactive species contributing to the photocatalytic degradation of the E3 hormone. On the other hand, introducing PBQ to the system led to total photodegradation of E3 hormone within a 2 h interval, which was faster than without any scavenger. Such enhanced photocatalytic efficiency could be related to decreased backward charge recombination. The obtained radical scavenging tests are slightly different from some other previously reported studies on ZnO/Ag, in which a significant contribution from superoxide anion ($^{\bullet}O^{2-}$) was also observed besides holes and $^{\bullet}OH$ (Singh, 2022; Zhu et al., 2021). Considering the above-mentioned scavenger results, a photocatalytic reaction mechanism is also drawn in Fig. 6, where the contribution from each ROS for redox reactions is highlighted.

For any viable photocatalytic system, it is imperative that as-prepared samples should maintain a high degree of performance over several cyclic usage. For that purpose, we subjected the best-performing sample, i.e., $ZnO_{nr/ncw}/Ag$, to five consecutive cyclic runs, which revealed that the sample was able to maintain high performance for E3 degradation, as shown in Fig. S6. The $ZnO_{nr/ncw}/Ag$ tested for reusability was further characterized with SEM and XRD to discern any structural or morphological changes. As can be deduced from Fig. S7 and Fig. S8 high structural integrity was maintained, and negligible change was observed in both morphology and XRD diffractogram. This study provides useful insights into developing environmentally friendly photocatalytic wastewater treatment for emerging environmental pollutants by considering aspects of circular economy and environmental sustainability.

3. Conclusions

Bioinspired Anelosimus eximius morphology design of 1D nanostructured ZnO, possessing nanorods/nano cobweb geometric configurations resembling the spider cobwebs, was successfully grown onto a glass substrate. The fine-tuning of the morphology was enabled by varying the molecular weight of polyethyleneimine (PEI), and the performance of this design was further enhanced by decorating the structures with silver (Ag) nanoparticles via the photoreduction method.

A preliminary evaluation of the photocatalytic activity of the surface according to the ISO 21066:2018 standard showed that the photocatalytic activity of the $ZnO_{nr/ncw}$ and $ZnO_{nr/ncw}/Ag$ samples initiated very quickly, within a few seconds of exposure to UV light. In addition, the films exhibited increased wettability upon UV irradiation, in the order $ZnO_{nr/ncw} > ZnO_{nr/ncw}/Ag > ZnO_{nr}$-KOH, making the samples ideal for self-cleaning applications.

From an environmental sustainability perspective, 1D hierarchical ZnO-based nanostructures were evaluated for the photodegradation of commonly prescribed drugs, such as carbamazepine and diclofenac sodium salt, which frequently contaminate wastewater. The highest photodegradation rate constants were obtained using the $ZnO_{nr/ncw}/Ag$ structures, which were 3.6 and 2.6 times greater for diclofenac and

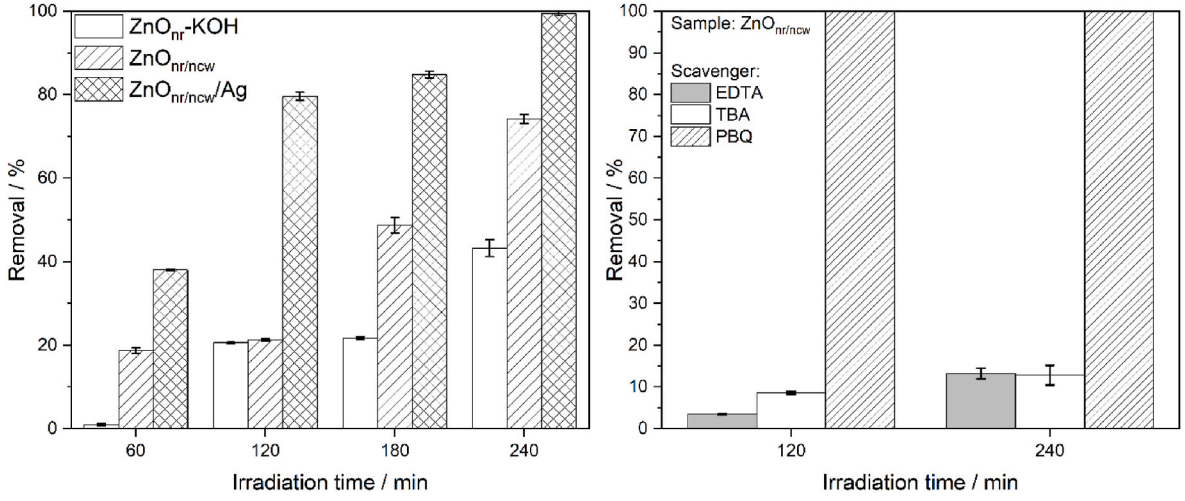

Fig. 5. Photodegradation rate of estriol hormone using as-prepared samples (left) and radical quenching results obtained with $ZnO_{nr/ncw}$ sample.

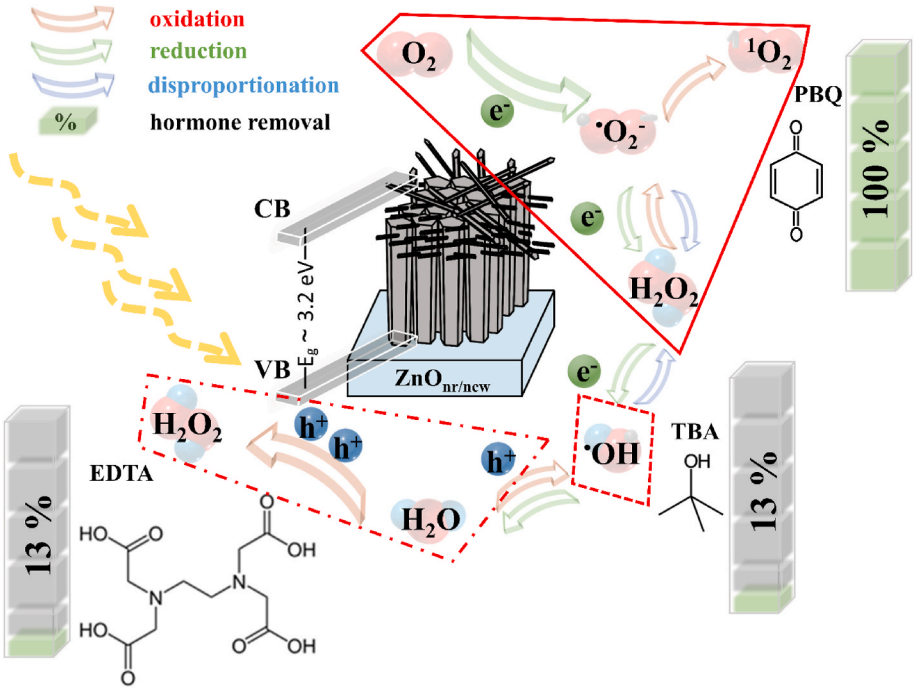

Fig. 6. Photocatalytic reaction mechanism of $ZnO_{nr/ncw}$ sample according to radical scavenging results.

carbamazepine, respectively, compared to the sample without Ag decoration ($ZnO_{nr/ncw}$), and 23.4 and 11.8 times greater than those for the etched sample, ZnO_{nr}-KOH.

The feasibility of the developed samples was tested in a model photoreactor using a continuous drop-flow mode of the liquid film over the coated surface. The estriol (E3) hormone was used as a representative pollutant of highly biotoxic and bioaccumulative endocrine disruptors, for which total elimination rates of 100%, 75%, and 50% were achieved for the samples $ZnO_{nr/ncw}$/Ag > $ZnO_{nr/ncw}$ > ZnO_{nr}-KOH within 4 h. The role of active species in photocatalytic activities was elucidated using radical scavenging tests. The holes and •OH radicals were identified as the primary reactive species involved in initiating the photocatalytic reaction for all prepared nanostructured ZnO thin films. The superior performance of the dual morphology (nanorods with nano cobwebs) Ag nanoparticle-decorated 1D ZnO nanostructures can be attributed to optimized charge transfer and separation in the heterostructure.

CRediT authorship contribution statement

Milan Masar: Writing – original draft, Methodology, Investigation, Formal analysis, Data curation. **Hassan Ali:** Writing – review & editing, Investigation, Formal analysis. **Muhammad Yasir:** Methodology, Investigation, Formal analysis. **Barbora Hanulikova:** Investigation, Formal analysis. **Orhan Sisman:** Investigation, Formal analysis. **Michal Zitnan:** Investigation, Formal analysis. **Michal Machovsky:** Writing – review & editing, Supervision, Resources, Project administration, Funding acquisition, Conceptualization. **Jose J. Velazquez:** Writing – review & editing. **Dusan Galusek:** Writing – review & editing, Resources, Project administration, Funding acquisition. **Ivo Kuritka:** Writing – review & editing, Supervision, Resources, Project administration, Methodology, Funding acquisition.

Declaration of competing interest

The authors declare that they have no known competing financial interests or personal relationships that could have appeared to influence the work reported in this paper.

Data availability

Data will be made available on request.

Acknowledgements

The authors gratefully acknowledge the financial support from the Ministry of Education, Youth, and Sports of the Czech Republic - INTER-EXCELLENCE (LTT20010) and DKRVO (RP/CPS/2024-28/007). The authors are also grateful for the funding received from the Internal Grant Agency (IGA) of TBU in Zlin (IGA/CPS/2023/006). H.A. and M.Y. also express their gratitude for support within the “Creativity, Intelligence & Talent for the Zlín Region” (CIT - ZK) program. Also, this work is a part of the dissemination activities of the FunGlass project. This project has received funding from the European Union’s Horizon 2020 research and innovation program under grant agreement No 739566. This work was also supported by the Slovak Research and Development Agency under grant VEGA 1/0844/21.

Appendix A. Supplementary data

Supplementary data to this article can be found online at https://doi.org/10.1016/j.chemosphere.2024.143327.

References

Abdulrahman, A.F., Ahmed, S.M., Hamad, S.M., Almessiere, M.A., Ahmed, N.M., Sajadi, S.M., 2021. Effect of different pH values on growth solutions for the ZnO nanostructures. Chin. J. Phys. 71, 175–189. https://doi.org/10.1016/J.CJPH.2021.02.013.

Al-Hajji, L.A., Ismail, A.A., Bumajdad, A., Alsaidi, M., Ahmed, S.A., Al-Hazza, A., Ahmed, N., 2021. Photodegradation of powerful five estrogens collected from waste water treatment plant over visible-light-driven Au/TiO_2 photocatalyst. Environ. Technol. Innov. 24, 101958 https://doi.org/10.1016/J.ETI.2021.101958.

Ansari, A.R., Hussain, S., Imran, M., Al-Ghamdi, A.A., Chandan, M.R., 2018. Optical investigations of microwave induced synthesis of zinc oxide thin-film. Materials Science- Poland 36, 304–309. https://doi.org/10.1515/MSP-2018-0041.

Ayalew, Z.M., Guo, X., Zhang, X., 2022. Synthesis and application of polyethyleneimine (PEI)-based composite/nanocomposite material for heavy metals removal from wastewater: a critical review. Journal of Hazardous Materials Advances 8, 100158. https://doi.org/10.1016/j.hazadv.2022.100158.

Ayesha, Imran, M., Haider, A., Shahzadi, I., Moeen, S., Ul-Hamid, A., Nabgan, W., Shahzadi, A., Alshahrani, T., Ikram, M., 2023. Polyvinylpyrrolidone and chitosan-coated magnetite (Fe_3O_4) nanoparticles for catalytic and antimicrobial activity with molecular docking analysis. J. Environ. Chem. Eng. 11, 110088 https://doi.org/10.1016/j.jece.2023.110088.

Bazant, P., Kuritka, I., Munster, L., Kalina, L., 2015. Microwave solvothermal decoration of the cellulose surface by nanostructured hybrid Ag/ZnO particles: a joint XPS, XRD and SEM study. Cellulose 22, 1275–1293. https://doi.org/10.1007/S10570-015-0561-Y.

Chang, J. Sen, Strunk, J., Chong, M.N., Poh, P.E., Ocon, J.D., 2020. Multi-dimensional zinc oxide (ZnO) nanoarchitectures as efficient photocatalysts: what is the fundamental factor that determines photoactivity in ZnO? J. Hazard Mater. 381, 120958 https://doi.org/10.1016/J.JHAZMAT.2019.120958.

Chen, C., Zheng, Y., Zhan, Y., Lin, X., Zheng, Q., Wei, K., 2011. Enhanced Raman scattering and photocatalytic activity of Ag/ZnO heterojunction nanocrystals. Dalton Trans. 40, 9566–9570. https://doi.org/10.1039/C1DT10799B.

Ching, C.G., Ooi, P.K., Ng, S.S., Ahmad, M.A., Hassan, Z., Abu Hassan, H., Abdullah, M.J., 2013. Fabrication of porous ZnO via electrochemical etching using 10 wt% potassium hydroxide solution. Mater. Sci. Semicond. Process. 16, 70–76. https://doi.org/10.1016/J.MSSP.2012.06.017.

Choi, S.M., Yoo, S.D., Lee, B.M., 2004. Toxicological characteristics of endocrine-disrupting chemicals: developmental toxicity, carcinogenicity, and mutagenicity. J. Toxicol. Environ. Health, Part A B 7, 1–32. https://doi.org/10.1080/716100635.

Ding, L., Zhou, H., Lou, S., Ding, J., Zhang, D., Zhu, H., Fan, T., 2013. Butterfly wing architecture assisted CdS/Au/TiO_2 Z-scheme type photocatalytic water splitting. Int. J. Hydrogen Energy 38, 8244–8253. https://doi.org/10.1016/J.IJHYDENE.2013.04.093.

Durán, A., Monteagudo, J.M., Expósito, A.J., Monsalve, V., 2016. Modeling the sonophoto-degradation/mineralization of carbamazepine in aqueous solution. Chem. Eng. J. 284, 503–512. https://doi.org/10.1016/J.CEJ.2015.09.016.

El-Shaer, A., Abdelfatah, M., Basuni, A., Mosaad, M., 2018. Effect of KOH molarity and annealing temperature on ZnO nanostructure properties. Chin. J. Phys. 56, 1001–1009. https://doi.org/10.1016/J.CJPH.2018.03.015.

Ensano, B.M.B., Borea, L., Naddeo, V., Belgiorno, V., de Luna, M.D.G., Ballesteros, F.C., 2017. Removal of pharmaceuticals from wastewater by intermittent electrocoagulation. Water 9, 85. https://doi.org/10.3390/W9020085, 85 9.

Frankcombe, T.J., Liu, Y., 2023. Interpretation of oxygen 1s X-ray photoelectron spectroscopy of ZnO. Chem. Mater. 35, 5468–5474. https://doi.org/10.1021/ACS.CHEMMATER.3C00801.

Ganguli, A.K., Kunde, G.B., Raza, W., Kumar, S., Yadav, P., 2022. Assessment of performance of photocatalytic nanostructured materials with varied morphology based on reaction conditions. Molecules 27, 7778. https://doi.org/10.3390/MOLECULES27227778.

Gao, X., Liu, X., Zhu, Z., Gao, Y., Wang, Q., Zhu, F., Xie, Z., 2017. Enhanced visible light photocatalytic performance of CdS sensitized TiO_2 nanorod arrays decorated with Au nanoparticles as electron sinks. Sci. Rep. 7, 1–10. https://doi.org/10.1038/s41598-017-01124-5.

García-Prieto, J.C., González-Burciaga, L.A., Proal-Nájera, J.B., García-Roig, M., 2022. Study of influence factors in the evaluation of the performance of a photocatalytic fibre reactor (TiO_2/SiO_2) for the removal of organic pollutants from water. Catalysts 12, 122. https://doi.org/10.3390/CATAL12020122.

Ghosh, A., Tripathy, A., Ghosh, D., 2022. Impact of endocrine disrupting chemicals (EDCs) on reproductive health of human. Proc. Zool. Soc. 75, 16–30. https://doi.org/10.1007/S12595-021-00412-3.

Gil, J.J., Aguilar-Martínez, O., Piña-Pérez, Y., Pérez-Hernández, R., Santolalla-Vargas, C. E., Gómez, R., Tzompantzi, F., 2020. Efficient ZnS–ZnO/ZnAl-LDH composite for H_2 production by photocatalysis. Renew. Energy 145, 124–132. https://doi.org/10.1016/j.renene.2019.06.001.

Grzegorzek, M., Wartalska, K., Kaźmierczak, B., 2023. Review of water treatment methods with a focus on energy consumption. Int. Commun. Heat Mass Tran. 143, 106674 https://doi.org/10.1016/J.ICHEATMASSTRANSFER.2023.106674.

Haddaoui, I., Mateo-Sagasta, J., 2021. A review on occurrence of emerging pollutants in waters of the MENA region. Environ. Sci. Pollut. Control Ser. 28, 68090–68110. https://doi.org/10.1007/s11356-021-16558-8.

Han, J., Liu, Y., Singhal, N., Wang, L., Gao, W., 2012. Comparative photocatalytic degradation of estrone in water by ZnO and TiO_2 under artificial UVA and solar irradiation. Chem. Eng. J. 213, 150–162. https://doi.org/10.1016/J.CEJ.2012.09.066.

Han, X.G., He, H.Z., Kuang, Q., Zhou, X., Zhang, X.H., Xu, T., Xie, Z.X., Zheng, L.S., 2009. Controlling morphologies and tuning the related properties of nano/microstructured ZnO crystallites. J. Phys. Chem. C 113, 584–589. https://doi.org/10.1021/JP808233E.

Hansen, M., Truong, J., Szychowski, B., Xie, T., Daniel, M.C., Hahm, J.I., 2019. Single nanomaterial level investigation of ZnO nanorod sulfidation reactions via position resolved confocal Raman spectroscopy. Nanoscale 11, 1147–1158. https://doi.org/10.1039/C8NR06039H.

Idriss, H., 2021. On the wrong assignment of the XPS O1s signal at 531–532 eV attributed to oxygen vacancies in photo- and electro-catalysts for water splitting and other materials applications. Surf. Sci. 712, 121894 https://doi.org/10.1016/j.susc.2021.121894.

Ikram, M., Moeen, S., Haider, A., Ul-Hamid, A., Alhummiany, H., Somaily, H.H., Goumri-Said, S., Kanoun, M.B., 2023. Experimental and computational study of annealed nickel sulfide quantum dots for catalytic and antibacterial activity. Nano Materials Science. https://doi.org/10.1016/j.nanoms.2023.11.007.

Kalaiarasan, S., Uthirakumar, P., Shim, D., Lee, I.H., 2021. The degradation profile of high molecular weight textile reactive dyes: a daylight induced photocatalytic activity of ZnO/carbon quantum dot photocatalyst. Environ. Nanotechnol. Monit. Manag. 15, 100423 https://doi.org/10.1016/J.ENMM.2020.100423.

Krzywiecki, M., Grządziel, L., Sarfraz, A., Iqbal, D., Szwajca, A., Erbe, A., 2015. Zinc oxide as a defect-dominated material in thin films for photovoltaic applications – experimental determination of defect levels, quantification of composition, and construction of band diagram. Phys. Chem. Chem. Phys. 17, 10004–10013. https://doi.org/10.1039/C5CP00112A.

Kumar, M., Sarma, D.K., Shubham, S., Kumawat, M., Verma, V., Prakash, A., Tiwari, R., 2020. Environmental endocrine-disrupting chemical exposure: role in non-communicable diseases. Front. Public Health. 8, 553850. https://doi.org/10.3389/fpubh.2020.553850.

Kusiak-Nejman, E., Ćmielewska, K., Wanag, A., Ekiert, E., Pełech, I., Narkiewicz, U., Morawski, A.W., 2023. Effect of TiO_2 crystallinity on the photocatalytic reduction of nitrogen and carbon dioxide. Appl. Catal. Gen. 657, 119164 https://doi.org/10.1016/J.APCATA.2023.119164.

Li, X., Chen, Y., Tao, Y., Shen, L., Xu, Z., Bian, Z., Li, H., 2022. Challenges of photocatalysis and their coping strategies. Chem Catal. 2, 1315–1345. https://doi.org/10.1016/J.CHECAT.2022.04.007.

Lin, D., Wu, H., Zhang, R., Pan, W., 2009. Enhanced photocatalysis of electrospun Ag-ZnO heterostructured nanofibers. Chem. Mater. 21, 3479–3484. https://doi.org/10.1021/CM900225P.

Liu, H., Zhong, L., Govindaraju, S., Yun, K., 2019a. ZnO rod decorated with Ag nanoparticles for enhanced photocatalytic degradation of methylene blue. J. Phys. Chem. Solid. 129, 46–53. https://doi.org/10.1016/J.JPCS.2018.12.040.

Liu, Y., Zhang, Q., Xu, M., Yuan, H., Chen, Y., Zhang, Jiaxi, Luo, K., Zhang, Jingquan, You, B., 2019b. Novel and efficient synthesis of Ag-ZnO nanoparticles for the sunlight-induced photocatalytic degradation. Appl. Surf. Sci. 476, 632–640. https://doi.org/10.1016/J.APSUSC.2019.01.137.

Lv, S., Du, Y., Wu, F., Cai, Y., Zhou, T., 2022. Review on LSPR assisted photocatalysis: effects of physical fields and opportunities in multifield decoupling. Nanoscale Adv. 4, 2608–2631. https://doi.org/10.1039/D2NA00140C.

Majeed, I., Ali, H., Idrees, A., Arif, A., Ashraf, W., Rasul, S., Khan, M.A., Nadeem, Muhammad Arif, Nadeem, Muhammad Amtiaz, 2022. Understanding the role of metal supported on TiO_2 in photoreforming of oxygenates. Energy Advances 1, 842–867. https://doi.org/10.1039/D2YA00110A.

Manghnani, M.H., Hushur, A., Sekine, T., Wu, J., Stebbins, J.F., Williams, Q., 2011. Raman, Brillouin, and nuclear magnetic resonance spectroscopic studies on shocked borosilicate glass. J. Appl. Phys. 109 https://doi.org/10.1063/1.3592346.

Manríquez, M.E., Morales-Mendoza, G., Alamilla, J., Trejo, U., Gómez, R., Ortiz-Islas, E., 2017. Photocatalytic oxidative esterification of benzaldehyde by V_2O_5–ZnO catalysts. React. Kinet. Mech. Catal. 122, 1281–1296. https://doi.org/10.1007/s11144-017-1262-3.

Masar, M., Ali, H., Guler, A.C., Suly, P., Urbanek, P., Antos, J., Hanulikova, B., Machovsky, M., Kuritka, I., 2024. Unveiling significant impact of subtle atomic displacement from equilibrium position in crystal lattice on electronic properties and photocatalytic activity of ZnO. Mater. Today Chem. 38, 102136 https://doi.org/10.1016/j.mtchem.2024.102136.

Mishra, Kirti, Devi, N., Siwal, S., Gupta, V.K., Thakur, V.K., Mishra, K., Siwal, S.S., 2023. Hybrid semiconductor photocatalyst nanomaterials for energy and environmental applications: fundamentals, designing, and prospects. Adv Sustain Syst 7, 2300095. https://doi.org/10.1002/ADSU.202300095.

Moeen, S., Ikram, M., Haider, A., Haider, J., Ul-Hamid, A., Nabgan, W., Shujah, T., Naz, M., Shahzadi, I., 2022. Comparative study of sonophotocatalytic, photocatalytic, and catalytic activities of magnesium and chitosan-doped tin oxide quantum dots. ACS Omega 7, 46428–46439. https://doi.org/10.1021/acsomega.2c05133.

Mou, H., Song, C., Zhou, Y., Zhang, B., Wang, D., 2018. Design and synthesis of porous Ag/ZnO nanosheets assemblies as super photocatalysts for enhanced visible-light degradation of 4-nitrophenol and hydrogen evolution. Appl. Catal., B 221, 565–573. https://doi.org/10.1016/J.APCATB.2017.09.061.

Moulder, J.F., Chastain, J., 1992. Handbook of X-ray photoelectron spectroscopy: a reference book of standard spectra for identification and interpretation of XPS data. Physical Electronics Division, Perkin-Elmer Corporation.

Mugunthan, E., Saidutta, M.B., Jagadeeshbabu, P.E., 2019. Photocatalytic activity of ZnO-WO_3 for diclofenac degradation under visible light irradiation. J. Photochem. Photobiol. Chem. 383, 111993 https://doi.org/10.1016/J.JPHOTOCHEM.2019.111993.

Musa, I., Qamhieh, N., Mahmoud, S.T., 2017. Synthesis and length dependent photoluminescence property of zinc oxide nanorods. Results Phys. 7, 3552–3556. https://doi.org/10.1016/j.rinp.2017.09.035.

Nath, D., Singh, F., Das, R., 2020. X-ray diffraction analysis by Williamson-Hall, Halder-Wagner and size-strain plot methods of CdSe nanoparticles- a comparative study. Mater. Chem. Phys. 239, 122021 https://doi.org/10.1016/J.MATCHEMPHYS.2019.122021.

National Institute of Standards and Technology, 2000. NIST X-Ray Photoelectron Spectroscopy Database. n.d. National Institute of Standards and Technology, Gaithersburg MD, 20899. https://doi.org/10.18434/T4T88K [WWW Document].

Nundy, S., Ghosh, A., Mallick, T.K., 2020. Hydrophilic and superhydrophilic self-cleaning coatings by morphologically varying ZnO microstructures for photovoltaic and glazing applications. ACS Omega 5, 1033–1039. https://doi.org/10.1021/ACSOMEGA.9B02758.

Nure, J.F., Nkambule, T.T.I., 2023. The recent advances in adsorption and membrane separation and their hybrid technologies for micropollutants removal from wastewater. J. Ind. Eng. Chem. 126, 92–114. https://doi.org/10.1016/J.JIEC.2023.06.034.

Ortúzar, M., Esterhuizen, M., Olicón-Hernández, D.R., González-López, J., Aranda, E., 2022. Pharmaceutical pollution in aquatic environments: a concise review of environmental impacts and bioremediation systems. Front. Microbiol. 13, 869332 https://doi.org/10.3389/FMICB.2022.869332.

Perdomo, C., Nguyen, N.T., 2022. Recent advances in 1D nanostructured catalysts for photothermal and photocatalytic reduction of CO_2. Curr. Opin. Colloid Interface Sci. 61, 101625 https://doi.org/10.1016/J.COCIS.2022.101625.

Petryayeva, E., Krull, U.J., 2011. Localized surface plasmon resonance: nanostructures, bioassays and biosensing—a review. Anal. Chim. Acta 706, 8–24. https://doi.org/10.1016/J.ACA.2011.08.020.

Pham, T.H., Viet, N.M., Hoai, P.T.T., Tung, N.H., Tran, H.M., Mapari, M.G., Kim, T., 2023. Synthesis of solar-driven Cu-doped graphitic carbon nitride photocatalyst for enhanced removal of caffeine in wastewater. Environ. Res. 233, 116483 https://doi.org/10.1016/j.envres.2023.116483.

Piña-Pérez, Y., Aguilar-Martínez, O., Acevedo-Peña, P., Santolalla-Vargas, C.E., Oros-Ruíz, S., Galindo-Hernández, F., Gómez, R., Tzompantzi, F., 2018. Novel ZnS-ZnO composite synthesized by the solvothermal method through the partial sulfidation of ZnO for H2 production without sacrificial agent. Appl. Catal., B 230, 125–134. https://doi.org/10.1016/j.apcatb.2018.02.047.

Preeti, K., Kumar, A., Jain, N., Kaushik, A., Mishra, Y.K., Sharma, S.K., 2023. Tailored ZnO nanostructures for efficient sensing of toxic metallic ions of drainage systems. Materials Today Sustainability 24, 100515. https://doi.org/10.1016/J.MTSUST.2023.100515.

Qin, J., Chu, K., Huang, Y., Zhu, X., Hofkens, J., He, G., Parkin, I.P., Lai, F., Liu, T., 2021. The bionic sunflower: a bio-inspired autonomous light tracking photocatalytic system. Energy Environ. Sci. 14, 3931–3937. https://doi.org/10.1039/D1EE00587A.

Qiu, J., Li, X., Zhuge, F., Gan, X., Gao, X., He, W., Park, S.-J., Kim, H.-K., Hwang, Y.-H., 2010. Solution-derived 40 μm vertically aligned ZnO nanowire arrays as photoelectrodes in dye-sensitized solar cells. Nanotechnology 21, 195602. https://doi.org/10.1088/0957-4484/21/19/195602.

Ranjith, K.S., Kruthika, B.S., Rajendrakumar, R.T., 2013. Synthesis and characterization of ZnO micro-tubes. Adv Mat Res 678, 217–222. https://doi.org/10.4028/WWW.SCIENTIFIC.NET/AMR.678.217.

Rhomberg, L.R., Seeley, M., Verslycke, T., Goodman, J.E., 2014. Environmental hormone disruptors. Encyclopedia of Toxicology 378–380. https://doi.org/10.1016/B978-0-12-386454-3.01010-1. Third Edition.

Ribut, S.H., Che Abdullah, C.A., Mohammad Yusoff, M.Z., 2019. Investigations of structural and optical properties of zinc oxide thin films growth on various substrates. Results Phys. 13, 102146 https://doi.org/10.1016/J.RINP.2019.02.082.

Römer, L., Scheibel, T., 2008. The elaborate structure of spider silk. Prion 2, 154–161. https://doi.org/10.4161/PRI.2.4.7490.

Sawant, S.Y., Kim, J.Y., Han, T.H., Ansari, S.A., Cho, M.H., 2018. Electrochemically active biofilm-assisted biogenic synthesis of an Ag-decorated ZnO@C core–shell ternary plasmonic photocatalyst with enhanced visible-photocatalytic activity. New J. Chem. 42, 1995–2005. https://doi.org/10.1039/C7NJ03936K.

Semalti, P., Saroha, J., Tawale, J.S., Sharma, S.N., 2023. Visible-light driven noble metal (Au, Ag) permeated multicomponent Cu_2ZnSnS_4 nanocrystals: a potential low-cost photocatalyst for textile effluents and heavy metal removal. Environ. Res. 217, 114875 https://doi.org/10.1016/j.envres.2022.114875.

Shaheen, F., Imran, M., Haider, A., Shahzadi, A., Moeen, S., Ul-Hamid, A., Ullah, H., Khan, S., Alshomrany, A.S., Jeridi, M., Al-Anazy, M. mana, Ikram, M., 2024. Size-controlled synthesis of La and chitosan doped cobalt selenide nanostructures for catalytic and antibacterial activity with molecular docking analysis. Int. J. Biol. Macromol. 263, 130096 https://doi.org/10.1016/j.ijbiomac.2024.130096.

Shahzadi, A., Moeen, S., Khan, A.D., Haider, A., Haider, J., Ul-Hamid, A., Nabgan, W., Shahzadi, I., Ikram, M., Al-Shanini, A., 2023. La-doped CeO quantum dots: novel dye degrader, antibacterial activity, and in silico molecular docking analysis. ACS Omega 8, 8605–8616. https://doi.org/10.1021/acsomega.2c07753.

Shandilya, P., Sambyal, S., Sharma, R., Mandyal, P., Fang, B., 2022. Properties, optimized morphologies, and advanced strategies for photocatalytic applications of WO_3 based photocatalysts. J. Hazard Mater. 428, 128218 https://doi.org/10.1016/J.JHAZMAT.2022.128218.

Sharma, J., Dhiman, P., Kumar, A., Sharma, G., 2024. Advances in photocatalytic NO oxidation by Z-scheme heterojunctions. Environ. Res. 240, 117431 https://doi.org/10.1016/j.envres.2023.117431.

Singh, S., 2022. Natural sunlight driven photocatalytic performance of Ag/ZnO nanocrystals. Mater. Today Commun. 33, 104438 https://doi.org/10.1016/J.MTCOMM.2022.104438.

Sudrajat, H., Babel, S., 2019. Loading of metallic silver onto ZnO for enhancement of electron population and photocatalytic activity. Optik 183, 472–482. https://doi.org/10.1016/J.IJLEO.2019.02.129.

Yadav, A.K., Singh, P., 2015. A review of the structures of oxide glasses by Raman spectroscopy. RSC Adv. 5, 67583–67609. https://doi.org/10.1039/C5RA13043C.

Yang, L., Fan, D., Li, Z., Cheng, Y., Yang, X., Zhang, T., 2022. A review on the bioinspired photocatalysts and photocatalytic systems. Adv Sustain Syst 6, 2100477. https://doi.org/10.1002/ADSU.202100477.

Yao, C., Lin, J., Wu, L., Li, L., Xu, N., Sun, J., Wu, J., 2021. High-visible-light photocatalytic activity of ZnO–Au nanocomposites synthesized by a controlled hydrothermal method. physica status solidi (a) 218, 2100150. https://doi.org/10.1002/PSSA.202100150.

Zhu, L.Y., Ou, L.X., Mao, L.W., Wu, X.Y., Liu, Y.P., Lu, H.L., 2023. Advances in noble metal-decorated metal oxide nanomaterials for chemiresistive gas sensors: overview. Nano-Micro Lett. 15, 1–75. https://doi.org/10.1007/S40820-023-01047-Z.

Zhu, X., Wang, J., Yang, D., Liu, J., He, L., Tang, M., Feng, W., Wu, X., 2021. Fabrication, characterization and high photocatalytic activity of Ag–ZnO heterojunctions under UV-visible light. RSC Adv. 11, 27257–27266. https://doi.org/10.1039/D1RA05060E.